Graphene Hot Paper

International Edition: DOI: 10.1002/anie.201913578
German Edition: DOI: 10.1002/ange.201913578

Concise, Single-Step Synthesis of Sulfur-Enriched Graphene: Immobilization of Molecular Clusters and Battery Applications

Haruka Omachi, Tsukasa Inoue, Shuya Hatao, Hisanori Shinohara, Alejandro Criado, Hirofumi Yoshikawa,* Zois Syrgiannis,* and Maurizio Prato**

Abstract: *The concise synthesis of sulfur-enriched graphene for battery applications is reported. The direct treatment of graphene oxide (GO) with the commercially available Lawesson's reagent produced sulfur-enriched-reduced GO (S-rGO). Various techniques, such as X-ray photoelectron spectroscopy (XPS), confirmed the occurrence of both sulfur functionalization and GO reduction. Also fabricated was a nanohybrid material by using S-rGO with polyoxometalate (POM) as a cathode-active material for a rechargeable battery. Transmission electron microscopy (TEM) revealed that POM clusters were individually immobilized on the S-rGO surface. This battery, based on a POM/S-rGO complex, exhibited greater cycling stability for the charge-discharge process than a battery with nanohybrid materials positioned between the POM and nonenriched rGO. These results demonstrate that the use of sulfur-containing groups on a graphene surface can be extended to applications such as the catalysis of electrochemical reactions and electrodes in other battery systems.*

Introduction

Graphene, a novel two-dimensional sheet of sp^2-hybridized carbon atoms, is an attractive material for a variety of applications.[1–4] Given its properties, including a large surface area, high mechanical strength, high chemical stability, and excellent electrical conductivity, graphene is used as a conductive support material for metal clusters and nanoparticles in catalysis[5,6] and electrochemical applications.[7–10] As a more applicable graphene platform, reduced graphene oxide (rGO) has been widely used in aspects of large-scale production and solution processability.[11–14] Recently, we demonstrated that nanohybrid materials comprising rGO and related nanocarbon materials with polyoxometalate (POM) can exhibit excellent performance as a catalyst for water oxidation[15,16] and as a cathode-active material for molecular cluster batteries (MCBs).[17,18] A cooperative enhancement of the capacitor effects has been ascribed to the conductivity of rGO. However, in most reports, the immobilization of metal species on graphene has been accomplished by physical adsorption through van der Waals or electrostatic interactions.[19,20] Therefore, preventing leaching and aggregation of metal species is difficult, which degrades the cycle performance.

To achieve efficient immobilization of metal clusters, the introduction of sulfur-containing groups is a promising approach.[21–23] The formation of a strong metal–sulfur bond enables long-term stability of immobilized clusters on the support material. Despite numerous reports on the synthesis of sulfur-doped graphene under high-temperature conditions, including thermal annealing,[24–27] solvothermal synthesis,[28,29] and chemical vapor deposition,[30–33] only a few successful examples of covalently sulfur-enriched graphene were reported.[34] Wilson and Rourke reported the functionalization and chemical reduction of GO with *S*-potassium thioacetate.[35] The resulting thioethers were subsequently converted into a thiol group, and gold nanoparticles were successfully

[*] Prof. Dr. H. Omachi, T. Inoue, Prof. Dr. H. Shinohara
Department of Chemistry, Graduate School of Science, Nagoya University, Chikusa, Nagoya 464-8602 (Japan)
E-mail: omachi@chem.nagoya-u.ac.jp
Prof. Dr. H. Omachi
Research Center for Materials Science, Nagoya University
Chikusa, Nagoya, 464-8602 (Japan)
S. Hatao, Prof. Dr. H. Yoshikawa
Department of Nanotechnology for Sustainable Energy, School of Science and Technology, Kwansei Gakuin University
Sanda, 669-1337 (Japan)
E-mail: yoshikawah@kwansei.ac.jp
Dr. A. Criado, Prof. Dr. M. Prato
Carbon Bionanotechnology Group, CICbiomaGUNE
P° Miramón 182, 20014 Guipúzcoa (Spain)
E-mail: prato@units.it
Dr. Z. Syrgiannis, Prof. Dr. M. Prato
Center of Excellence for Nanostructured Materials (CENMAT), INSTM, Dipartimento di Scienze Chimiche e Farmanceutiche, Università di Trieste, Piazzale Europa, 1, 34127 Trieste (Italy)
E-mail: zois.syrgiannis@gmail.com
Prof. Dr. M. Prato
Basque Foundation for Science, Ikerbasque
Bilbao 48013 (Spain)
Dr. Z. Syrgiannis
Present Address: Simpson Querrey Institute
Northwestern University
303 East Superior Street, 11th floor, Chicago, IL 60611 (USA)
and
Department of Chemistry, Northwestern University
2145 Sheridan Road, Evanston, IL 60208 (USA)
Supporting information and the ORCID identification number(s) for the author(s) of this article can be found under: https://doi.org/10.1002/anie.201913578.

immobilized on thiolated rGO. Pumera and co-workers also reported the one-pot thiolation and reduction of GO by the use of thiourea and HBr followed by hydrolysis treatment.[36] However, both methods for the synthesis of sulfur-enriched graphene require deprotection steps to generate S–H groups, which can bind different metallic clusters.[37–39]

In the present study, we demonstrate direct and single-step synthesis of sulfur-enriched rGO (S-rGO) using Lawesson's reagent. Lawesson's reagent[40] is widely used for the conversion of both carbonyl and hydroxy groups into thiocarbonyl[41,42] and thiol[43] groups, respectively. However, Zhu and co-workers reported that the reduction of GO by treatment with Lawesson's reagent occurs only in toluene at 110 °C,[44] and the percentage of sulfur atoms increased by only 0.1 at. %. Recently, Tagmatarchis and co-workers reported the synthesis of S-doped graphene sheets with the use of Lawesson's reagent as a photoelectrocatalyst.[45] In our procedure, we used milder reaction conditions and we succeed in a high loading of sulfur on the final materials. The thionated GO materials have been incorporated with polyoxometalate clusters and were tested as battery cathode electrodes.

Results and Discussion

To achieve thiol functionalization of GO, the reaction conditions were optimized. In particular, three different methods were employed for the preparation of GO: the classical Hummer method,[46] the improved Hummer methods reported by Tour,[47] and the Nishina method.[48] After optimizing the reaction conditions, we succeeded in enhancing the amount of sulfur in the new graphitic material to approximately 10 % (depending on the type of GO that was used as the starting material, see Tables S1 in the Supporting Information). At the same time, we also observed a partial reduction of the GO. Eventually, we found that GO obtained by Nishina's method, in refluxing THF, produced the desired S-rGO, balancing the percentage of sulfur content with high conductivity (Scheme 1). To control the sulfur content and the degree of reduction, X-ray photoelectron spectroscopy (XPS) measurements were conducted (Figure 1). After having the best procedure for the preparation of high-sulfur-containing GO with the highest conductivity at the same time (see Table S2), we decided to focus on materials prepared with GO obtained by Nishina's method and the use of one

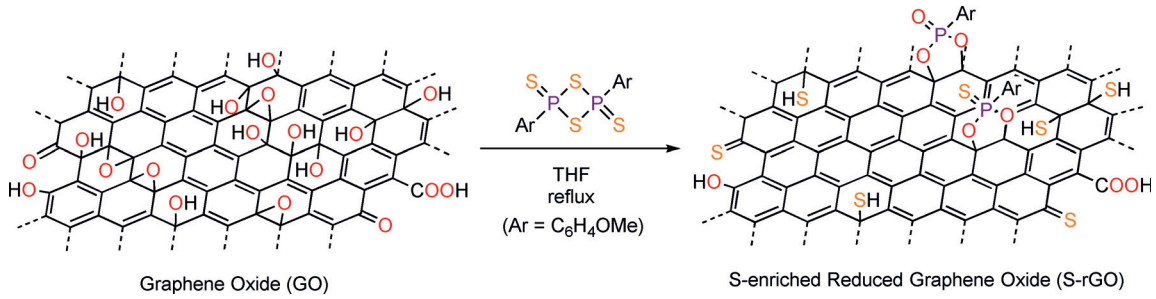

Scheme 1. Synthesis of sulfur-enriched-reduced GO (S-rGO).

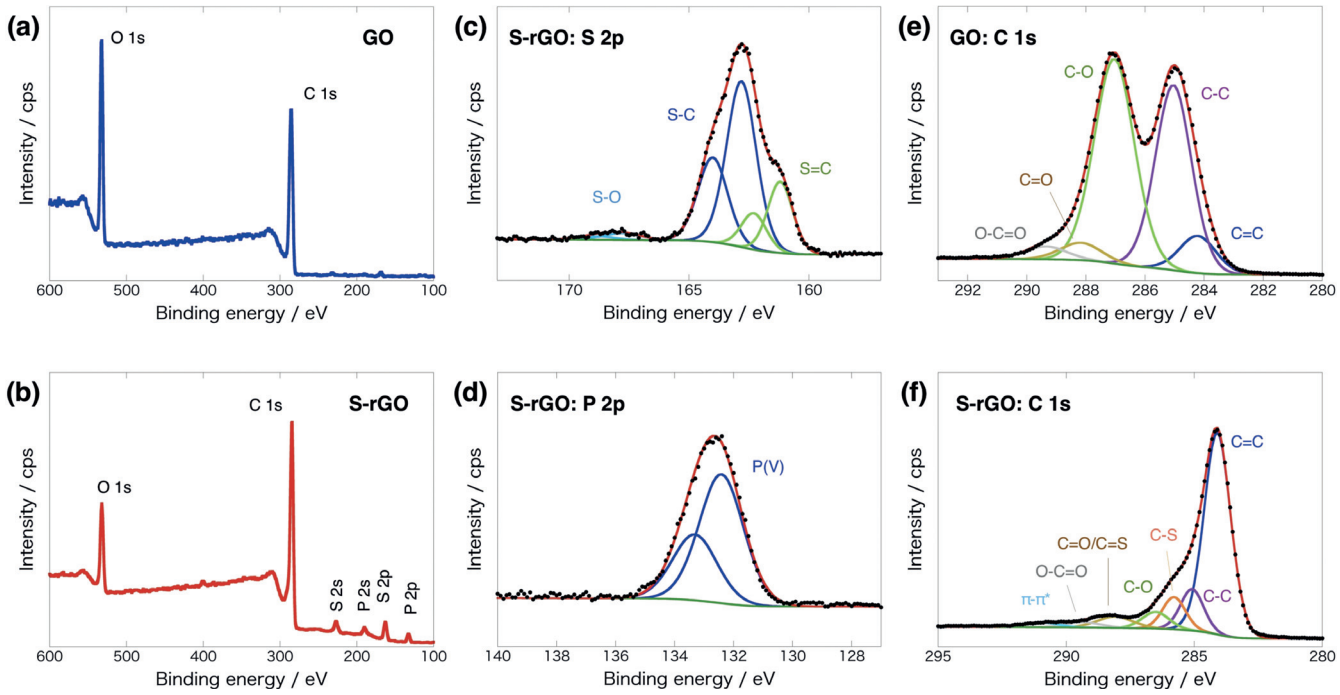

Figure 1. Survey XPS spectrum of GO (a) and S-rGO (b). S 2p (c) and P 2p (d) XPS spectra of S-rGO. C 1 s XPS spectra of GO (e) and S-rGO (f).

equivalent (in moles of carbon) of Lawesson's reagent. In addition to the distinct peaks for carbon 1s at 284 eV and oxygen 1s at 532 eV, the 2s and 2p peaks of sulfur (163 and 227 eV)[35,36] and phosphorus (2s: 190 eV, 2p: 133 eV)[49] were clearly present in the spectrum of the S-rGO sample. The elemental contents of sulfur and phosphorus atoms in S-rGO were 3.6 and 2.2 at. %, respectively (see Table S1). The sulfur content percentage is comparable to that of previous examples reported by Wilson and Rourke (ca. 4 at. %)[35] and Pumera (2.10 at. %).[36] The heteroatom contents were decreased by the reaction with H_2O additive to enhance retro-functionalization.[50]

A high-resolution (HR) spectrum of the S 2p region is shown in Figure 1c. After performing a $2p_{3/2}$-$2p_{1/2}$ doublet separation with 2:1 intensity, the major peaks can be assigned to the covalent C–S bond (162.8 and 164.0 eV)[36] and C=S bond (161.2 and 162.3 eV),[51] indicating the existence of thiol and thiocarbonyl moieties. Negligibly weak sulfoxide (S–O) peaks, caused by the oxidization of introduced sulfur, were also detected at about 168 eV. In contrast, the peak for pentavalent phosphorus atoms was only observed by HR-XPS measurements of phosphorus 2p (Figure 1d). To obtain a detailed structure, solid-state ^{31}P NMR measurements were conducted (see Figure S2). The spectrum shows two major peaks at $\delta = 9$ and 71 ppm, indicating the formation of phosphonate and thiophosphonate by the condensation reaction between thiophosphine ylides and hydroxy groups.[52,53]

The HR C 1s spectra of the original GO and the fitted peaks are shown in Figure 1e. The primary fitted peaks with binding energies of 285.0 and 287.1 eV can be ascribed to the carbon(sp^3)—carbon(sp^3) bond and single carbon–oxygen bond, respectively. This bonding results from the high abundance of hydroxy and epoxy groups and the honeycomb carbon network of GO. Although the fitted peaks originating from the C–S and C=S bonds were positioned at 285.8 and 288.1 eV, respectively, a significant decline in the C–O bond peak and a dominant graphitic C–C peak at 284.1 eV were observed in the C 1s spectra for S-rGO (Figure 1e). The peak intensity ratio of C=C/C–O was drastically changed from 0.17 to 3.2. Moreover, the oxygen content decreased from 29.9 to 13.7 at. % (see Table S1). These findings strongly indicate that together with the sulfur functionalization, a partial chemical reduction of GO occurred by using Lawesson's reagent.

The GO and S-rGO samples were also characterized by Fourier-transform infrared (FT-IR) and Raman spectroscopy to obtain further structural information (Figure 2). The FT-IR spectrum of GO (blue) contains three primary bands, assigned to O–H (3000–3670 cm^{-1}), C=O (1600–1750 cm^{-1}), and C–O (900–1450 cm^{-1}; Figure 2a). In the spectrum of S-rGO (red), these bands for oxygen-containing functional groups were weaker, and moderate peaks attributed to C=C bonds ($\approx$1500 cm^{-1}) were observed. Figure 2b shows the Raman spectra for GO (blue) and S-rGO (red). In both spectra, the two primary Raman peaks at approximately 1600 and 1350 cm^{-1} can be assigned to the G and D bands of graphene, respectively. After the reaction with Lawesson's reagent, the G-band peak shifted from 1602 to 1589 cm^{-1}, which is close to the typical value of rGO.[53,54] In addition, the

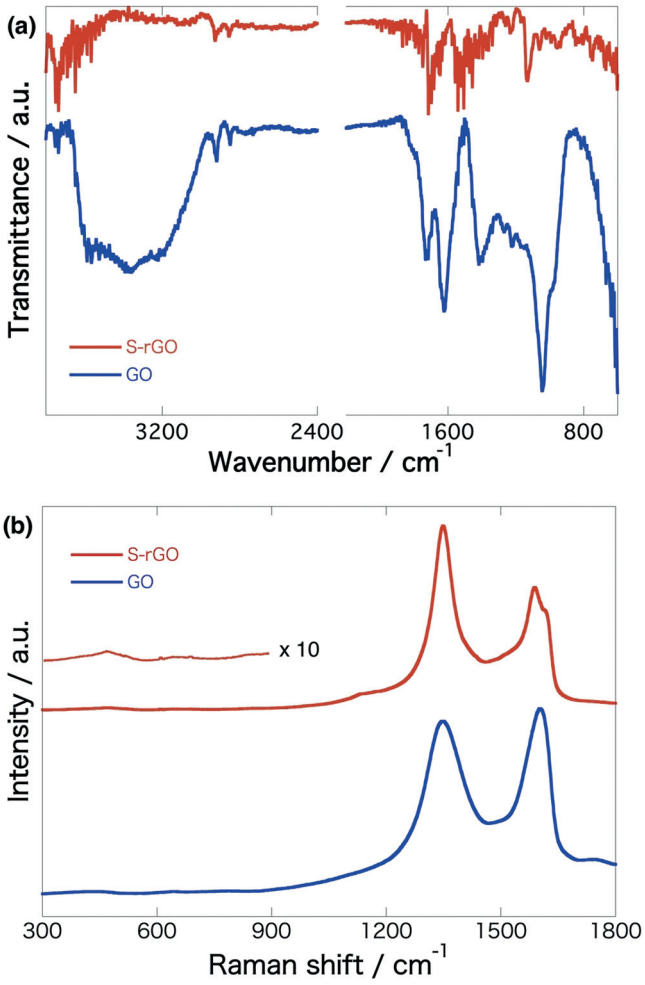

Figure 2. a) FT-IR and b) Raman spectra of GO (blue) and S-rGO (red).

full-width half maximum of the D band decreased from 148 to 58.6 cm^{-1}, strongly supporting the restoration of a symmetrical graphene structure.[54,55] Close to the G-band, a shoulder D′ band (1620 cm^{-1}) was observed in the Raman spectrum of S-rGO (Figure 2b). This peak indicates low symmetry of the graphene network,[56] which is caused by partial reduction resulting from the covalent bond formation with graphitic carbon atoms. The weak shoulder band at 1130 cm^{-1} and the broad peak at 468 cm^{-1} are attributed to C=S and C–S stretching vibrations, respectively. Furthermore, relatively sharp peaks at approximately 1132 cm^{-1} in the IR spectrum of S-rGO, shown in Figure 2a, were assigned to C=S bonds. These FT-IR and Raman results agree well with the XPS findings.

For a macroscopic analysis of the new materials, HR transmission electron macroscopy (HR-TEM) was used. From low-magnification TEM images of GO and S-rGO (Figures 3a,b), we confirmed that the S-rGO maintained a single- to few-layer structure with a large domain size. The surface of the S-rGO presents a more uniform contrast than that of GO, given the chemical reduction and the conversion of the wavy sp^3 form into a flat sp^2 network. High-magnification TEM images and corresponding electron

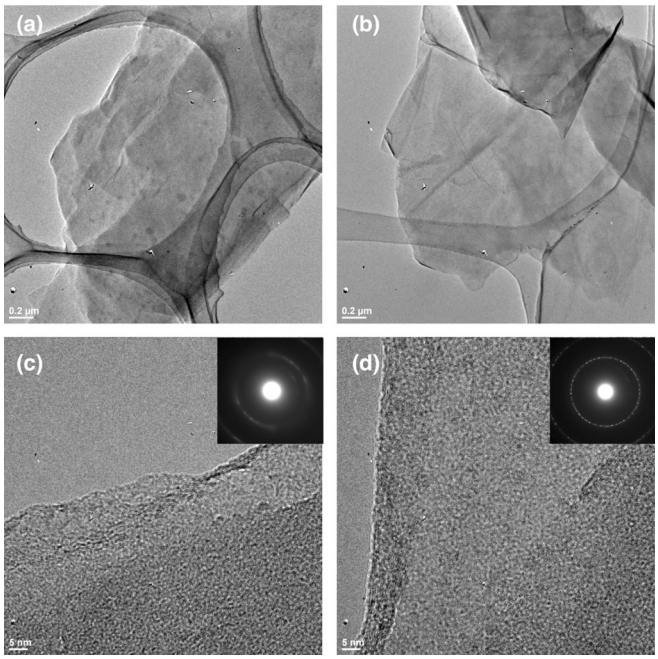

Figure 3. Typical low-magnification TEM images of GO (a) and S-rGO (b). High-magnification TEM images and diffraction patterns (inset) of GO (c) and S-rGO (d).

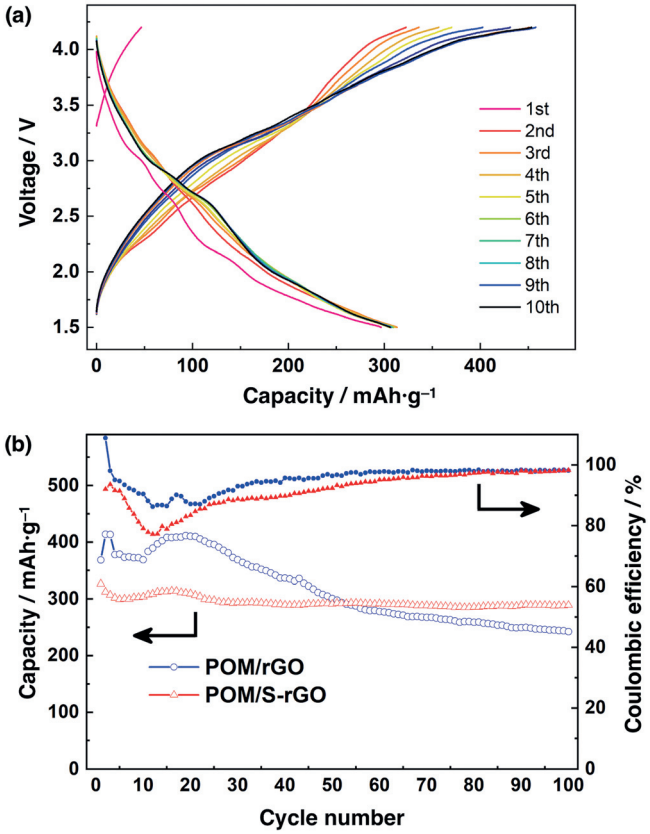

Figure 4. a) Charge-discharge curves of an MCB comprised of POM/S-rGO nanohybrid materials for the first 10 cycles. b) Cycle performance of the discharge capacities and Coulombic efficiencies at 1.5 V for MCBs comprised of POM/S-rGO (red) and POM/rGO (blue).

diffraction patterns are shown in Figures 3c and 3d. The diffuse diffraction ring pattern shown in the inset of Figure 3d indicates that the S-rGO exhibits a highly disordered graphene structure[33] resulting from the functionalization with sulfur- and phosphorus-containing groups. The existence of these heteroatoms was also confirmed by energy dispersive X-ray spectrometry (EDS) analysis (see Figure S3).

With S-rGO in hand, nanohybrid materials with POMs were prepared and used as cathode-active materials in lithium batteries to investigate potential applications of S-rGO. As mentioned above, Keggin-type POM[57,58] $TBA_3[PMo_{12}O_{40}]$ molecules were adsorbed onto S-rGO at a weight ratio of POM:S-rGO = 1:2. FT-IR and XPS measurements confirmed the successful interaction of S-rGO with POM based on the appearance of characteristic peaks of POM clusters after immobilization treatment (see Figures S4 and S5, and Table S3). After the preparation of these hybrid materials, we measured charge-discharge curves for a lithium battery composed of POM/S-rGO, where the capacity is given per unit weight of the POM in the nanohybrid materials, which occupy 10 wt% of the cathodes (Figure 4a). During the first charge process, the voltage quickly increases from the initial value (ca. 3.0 V) to 4.2 V because the POM clusters in the as-prepared nanohybrid materials are already in the charged state. The first discharge curve displays a gradual voltage decrease with a small plateau, which is similar to the finding for the POM/rGO samples (see Figure S6), with a high capacity of about 320 $mAh\,g^{-1}$ at 1.5 V. This value is larger than the previously reported value of about 260 $mAh\,g^{-1}$ for a POM cluster only, which can be explained by the reduction of Mo^{6+} to Mo^{4+} for the 12 molybdenum ions in the POM. As reported for the battery performance of POM/rGO[17] and POM/SWCNT[18] nanohybrid materials, researchers proposed that this excess capacity over the POM reduction is caused by the electrical double-layer capacitance formed at the interface between the POM and nanocarbons in the nanohybrid materials. However, the value is smaller than that for POM/rGO nanohybrid materials, indicating a smaller electrical double-layer capacitance for POM/S-rGO nanohybrid materials because of their lower conductivity ($2.5\times10^{2}\,S\,m^{-1}$) compared with that of rGO ($5.1\times10^{3}\,S\,m^{-1}$; see Table S2). In the charging process after the second cycle, the capacity gradually increased to the same level as the discharge value, indicating good reversible charge-discharge behavior. The cycle performance, as determined from the first 100 charge-discharge processes, is shown in Figure 4b. There is no significant decrease in capacity for the POM/S-rGO nanohybrid materials, while the discharge capacity of the POM/rGO materials gradually decreases and finally becomes smaller than that of the POM/S-rGO. A similar decrease in discharge capacity was confirmed for MCB comprising the nanohybrid materials using the low-sulfur-content S-rGO (see Figure S7). The Coulombic efficiency remains at nearly 100% after cycling.

To evaluate the cycle stability of MCBs using POM/S-rGO cathodes, HR-TEM observations of the nanohybrid materials were conducted. A typical TEM image of the POM/

S-rGO nanohybrid materials is shown in Figure 5a. The slightly dark contrast regions that are indicative of POM molecules, confirmed by EDS measurements (see Figure S8), were uniformly spread out on the S-rGO graphene sheet. In contrast, POM molecules were sparsely attached to the rGO surface (Figure 5b). The presence of strong dark contrast regions indicates large aggregates of POMs. The size distributions of the POMs on S-rGO or rGO are summarized in Figure 5c. The average diameter of POM molecules on the S-rGO sheet is 0.9 nm, which is consistent with the size of $PMo_{12}O_{40}$ clusters.[58] However, most POMs have a diameter greater than 1.5 nm in the case of the POM and rGO hybrid materials. Researchers suggested that this electrochemical stability of the POM and S-rGO is caused by a specific coordination of the individual POM clusters with S-rGO, which most likely produces Mo–S bonds that maintain the primary molecular structure, as indicated by XPS and Raman spectroscopy (see Figures S9 and S10).[59–61] The POM is not dissolved into the electrolyte, and thus, the redox reaction of POM and the electrochemical double-layer occurs in a stable and reversible manner. These results suggest that the increased conductivity of S-rGO may be beneficial for a much higher capacity as well as a cycling stability.

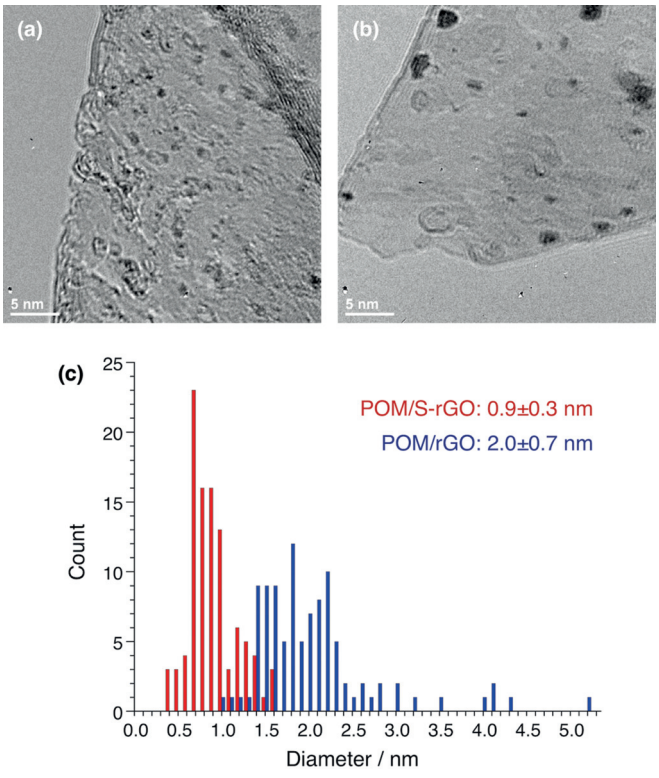

Figure 5. Typical HR-TEM images of POM/S-rGO (a) and POM/rGO (b) nanohybrid materials. c) Size distributions of POM on S-rGO (red) or rGO (blue).

Conclusion

In conclusion, the concise synthesis of S-rGO based on Lawesson's reagent was achieved. Spectroscopic analyses and microscopic observations revealed the reduction of GO and the effective functionalization with thiol, thiocalcarbonyl, and thiophosphonate groups. We also demonstrated the nanohybridization of S-rGO and POM clusters for use as a battery cathode material. POM clusters were individually immobilized on the S-rGO surface, and a lithium battery based on the POM and S-rGO complex exhibited high cycling stability for the charge-discharge process. Although the capacity of this battery was slightly lower than that for a battery including nanohybrid materials between the POM and simple rGO, this study demonstrated the importance of thiol groups on graphene for stable immobilization. The potential impact of sulfur-enriched graphene is unlimited. We believe that S-rGO can be applied to other metal clusters and nanoparticles for applications in the catalysis of electrochemical reactions and as fuel cell electrodes.

Experimental Section

Experimental and analytical details are given in the Supporting Information.

Acknowledgements

This work was financially supported by MEXT/JSPS KAKENHI (15K21073, 19K15539 to H.O., 16H06350, 16H02248 to H.S. and 18H04528, 17H03048, 18H04491 to H.Y.) and in part by research grants from Nippon Shokubai Co. Ltd., Kondo Zaidan, JGC-S Scholarship Foundation. We acknowledged financial support from the European Union's Horizon 2020 research and innovation program under Grant Agreements 696656 and 785219 Graphene Flagship. This work was also supported by the Spanish Ministry of Economy and Competitiveness MINECO (projects IJCI-2016-31113), by the University of Trieste, and Consorzio Interuniversitario Nazionale per la Scienza e Tecnologia dei Materiali (INSTM). MP, as the recipient of the AXA Chair, is grateful to the AXA Research Fund for financial support. This work was performed under the Maria de Maeztu Units of Excellence Program from the Spanish State Research Agency—Grant No. MDM-2017-0720. We also thank Prof. Yuta Nishina (Okayama University) for providing graphene oxide samples.

Conflict of interest

The authors declare no conflict of interest.

Keywords: cluster compounds · graphene · polyoxometalates · sulfur · surface chemistry

How to cite: *Angew. Chem. Int. Ed.* **2020**, *59*, 7836 – 7841
Angew. Chem. **2020**, *132*, 7910 – 7915

[1] K. S. Novoselov, A. K. Geim, S. V. Morozov, D. Jiang, Y. Zhang, S. V. Dubonos, I. V. Grigorieva, A. A. Firsov, *Science* **2004**, *306*, 666 – 669.
[2] A. K. Geim, K. S. Novoselov, *Nat. Mater.* **2007**, *6*, 183 – 191.
[3] A. K. Geim, *Science* **2009**, *324*, 1530 – 1534.
[4] K. S. Novoselov, V. I. Fal′ko, L. Colombo, P. R. Gellert, M. G. Schwab, K. Kim, *Nature* **2012**, *490*, 192 – 200.
[5] N. M. Julkapli, S. Bagheri, *Int. J. Hydrogen Energy* **2015**, *40*, 948 – 979.
[6] S. Navalon, A. Dhakshinamoorthy, M. Alvaro, H. Garcia, *Coord. Chem. Rev.* **2016**, *312*, 99 – 148.
[7] D. A. C. Brownson, D. K. Kampouris, C. E. Banks, *J. Power Sources* **2011**, *196*, 4873 – 4885.
[8] M. Liu, R. Zhang, W. Chen, *Chem. Rev.* **2014**, *114*, 5117 – 5160.
[9] R. Raccichini, A. Varzi, S. Passerini, B. Scrosati, *Nat. Mater.* **2015**, *14*, 271 – 279.
[10] M. P. Yu, R. Li, M. M. Wu, G. Q. Shi, *Energy Storage Mater.* **2015**, *1*, 51 – 73.
[11] S. Stankovich, D. A. Dikin, G. H. B. Dommett, K. M. Kohlhaas, E. J. Zimney, E. A. Stach, R. D. Piner, S. T. Nguyen, R. S. Ruoff, *Nature* **2006**, *442*, 282 – 286.
[12] O. C. Compton, S. T. Nguyen, *Small* **2010**, *6*, 711 – 723.
[13] C. K. Chua, M. Pumera, *Chem. Soc. Rev.* **2014**, *43*, 291 – 312.
[14] A. Montagner, S. Bosi, E. Tenori, M. Bidussi, A. A. Alshatwi, M. Tretiach, M. Prato, Z. Syrgiannis, *2D Mater.* **2016**, *4*, 012001.
[15] F. M. Toma, A. Sartorel, M. Iurlo, M. Carraro, P. Parisse, C. Maccato, S. Rapino, B. R. Gonzalez, H. Amenitsch, T. Da Ros, L. Casalis, A. Goldoni, M. Marcaccio, G. Scorrano, G. Scoles, F. Paolucci, M. Prato, M. Bonchio, *Nat. Chem.* **2010**, *2*, 826 – 831.
[16] M. Quintana, A. M. López, S. Rapino, F. M. Toma, M. Iurlo, M. Carraro, A. Sartorel, C. Maccato, X. Ke, C. Bittencourt, T. Da Ros, G. van Tendeloo, M. Marcaccio, F. Paolucci, M. Prato, M. Bonchio, *ACS Nano* **2013**, *7*, 811 – 817.
[17] K. Kume, N. Kawasaki, H. Wang, T. Yamada, H. Yoshikawa, K. Awaga, *J. Mater. Chem. A* **2014**, *2*, 3801 – 3807.
[18] N. Kawasaki, H. Wang, R. Nakanishi, S. Hamanaka, R. Kitaura, H. Shinohara, T. Yokoyama, H. Yoshikawa, K. Awaga, *Angew. Chem. Int. Ed.* **2011**, *50*, 3471 – 3474; *Angew. Chem.* **2011**, *123*, 3533 – 3536.
[19] D. Eder, *Chem. Rev.* **2010**, *110*, 1348 – 1385.
[20] A. Dolbecq, E. Dumas, C. R. Mayer, P. Mialane, *Chem. Rev.* **2010**, *110*, 6009 – 6048.
[21] A. N. Shipway, E. Katz, I. Willner, *ChemPhysChem* **2000**, *1*, 18 – 52.
[22] F. Caruso, *Adv. Mater.* **2001**, *13*, 11 – 22.
[23] E. Maria Claesson, A. P. Philipse, *Colloids Surf. A* **2007**, *297*, 46 – 54.
[24] J. Liang, Y. Jiao, M. Jaroniec, S. Z. Qiao, *Angew. Chem. Int. Ed.* **2012**, *51*, 11496 – 11500; *Angew. Chem.* **2012**, *124*, 11664 – 11668.
[25] Z. Yang, Z. Yao, G. Li, G. Fang, H. Nie, Z. Liu, X. Zhou, X. Chen, S. M. Huang, *ACS Nano* **2012**, *6*, 205 – 211.
[26] H. L. Poh, P. Simek, Z. Sofer, M. Pumera, *ACS Nano* **2013**, *7*, 5262 – 5272.
[27] S. Yang, L. Zhi, K. Tang, X. Feng, J. Maier, K. Müllen, *Adv. Funct. Mater.* **2012**, *22*, 3634 – 3640.
[28] Y. Yan, Y.-X. Yin, S. Xin, Y.-G. Guo, L.-J. Wan, *Chem. Commun.* **2012**, *48*, 10663 – 10665.
[29] D. Zheng, J. Zhang, W. Lv, T. Cao, S. Zhang, D. Qiu, Y. Tao, Y. He, F. Kang, Q.-H. Yang, *Chem. Commun.* **2018**, *54*, 4317 – 4320.
[30] W. Ai, Z. Luo, J. Jiang, J. Zhu, Z. Du, Z. Fan, L. Xie, H. Zhang, W. Huang, T. Yu, *Adv. Mater.* **2014**, *26*, 6186 – 6192.
[31] Y. Ito, W. Cong, T. Fujita, Z. Tang, M. Chen, *Angew. Chem. Int. Ed.* **2015**, *54*, 2131 – 2136; *Angew. Chem.* **2015**, *127*, 2159 – 2164.
[32] H. Liu, N. Kishi, T. Soga, *Mater. Lett.* **2015**, *159*, 114 – 117.
[33] F. Hassani, H. Tavakol, F. Keshavarzipour, A. Javaheri, *RSC Adv.* **2016**, *6*, 27158 – 27163.
[34] S. Kannappan, H. Yang, K. Kaliyappan, R. K. Manian, A. Samuthira Pandian, Y. S. Lee, J.-H. Jang, W. Lu, *Carbon* **2018**, *134*, 326 – 333.
[35] H. R. Thomas, A. J. Marsden, M. Walker, N. R. Wilson, J. P. Rourke, *Angew. Chem. Int. Ed.* **2014**, *53*, 7613 – 7618; *Angew. Chem.* **2014**, *126*, 7743 – 7748.
[36] C. K. Chua, M. Pumera, *ACS Nano* **2015**, *9*, 4193 – 4199.
[37] C. V. Pham, M. Eck, M. Krueger, *Chem. Eng. J.* **2013**, *231*, 146 – 154.
[38] J. Debgupta, V. K. Pillai, *Nanoscale* **2013**, *5*, 3615 – 3619.
[39] C. V. Pham, S. Repp, R. Thomann, M. Krueger, S. Weber, E. Erdem, *Nanoscale* **2016**, *8*, 9682 – 9687.
[40] H. Z. Lecher, R. A. Greenwood, K. C. Whitehouse, T. H. Chao, *J. Am. Chem. Soc.* **1956**, *78*, 5018.
[41] I. Thomsen, K. Clausen, S. Scheibye, S. O. Lawesson, *Org. Synth.* **1984**, *62*, 158.
[42] M. P. Cava, M. I. Levinson, *Tetrahedron* **1985**, *41*, 5061.
[43] T. Nishio, *J. Chem. Soc. Chem. Commun.* **1989**, 205 – 206.
[44] H. Liu, L. Zhang, Y. Guo, C. Cheng, L. Yang, L. Jiang, G. Yu, W. Hu, Y. Liu, D. Zhu, *J. Mater. Chem. C* **2013**, *1*, 3104 – 3109.
[45] A. Stergiou, D. K. Perivoliotis, N. Tagmatarchis, *Nanoscale* **2019**, *11*, 7335 – 7346.
[46] W. S. Hummers, R. E. Offeman, *J. Am. Chem. Soc.* **1958**, *80*, 1339.
[47] D. C. Marcano, D. V. Kosynkin, J. M. Berlin, A. Sinitskii, Z. Sun, A. Slesarev, L. B. Alemany, W. Lu, J. M. Tour, *ACS Nano* **2010**, *4*, 4806 – 4814.
[48] N. Morimoto, T. Kubo, Y. Nishina, *Sci. Rep.* **2016**, *6*, 25824.
[49] A. Rossi, F. M. Piras, D. Kim, A. J. Gellman, N. D. Spencer, *Tribol. Lett.* **2006**, *23*, 197 – 208.
[50] M. Jesberger, T. P. Davis, L. Barner, *Synthesis* **2003**, 1929 – 1958.
[51] J. Yang, D. Gong, G. Li, G. Zeng, Q. Wang, Y. Zhang, G. Liu, P. Wu, E. Vovk, Z. Peng, X. Zhou, Y. Yang, Z. Liu, Y. Sun, *Adv. Mater.* **2018**, *30*, 1705775.
[52] A. M. Puziy, O. I. Poddubnaya, R. P. Socha, J. Gurgul, M. Wisniewski, *Carbon* **2008**, *46*, 2113 – 2123.
[53] W. Przychodzeń, *Eur. J. Org. Chem.* **2005**, 2002 – 2014.
[54] S. Stankovich, D. A. Dikin, R. D. Piner, K. A. Kohlhaas, A. Kleinhammes, Y. Jia, Y. Wu, S. T. Nguyen, R. S. Ruoff, *Carbon* **2007**, *45*, 1558 – 1565.
[55] W. Chen, L. Yan, P. R. Bangal, *J. Phys. Chem. C* **2010**, *114*, 19885 – 19890.
[56] M. A. Pimenta, G. Dresselhaus, M. S. Dresselhaus, L. G. Cançado, A. Jorio, R. Saito, *Phys. Chem. Chem. Phys.* **2007**, *9*, 1276 – 1290.
[57] C. Sanchez, J. Livage, J. P. Launay, M. Fournier, Y. Jeannin, *J. Am. Chem. Soc.* **1982**, *104*, 3194 – 3202.
[58] H. Wang, S. Hamanaka, Y. Nishimoto, S. Irle, T. Yokoyama, H. Yoshikawa, K. Awaga, *J. Am. Chem. Soc.* **2012**, *134*, 4918 – 4924.
[59] P. D. Tran, T. V. Tran, M. Orio, S. Torelli, Q. D. Truong, K. Nayuki, Y. Sasaki, S. Y. Chiam, R. Yi, I. Honma, J. Barber, V. Artero, *Nat. Mater.* **2016**, *15*, 640 – 646.
[60] B. Zhu, Z.-L. Lang, N.-N. Ma, L.-K. Yan, Z.-M. Su, *Phys. Chem. Chem. Phys.* **2014**, *16*, 18017 – 18022.
[61] A. Popa, V. Sasca, D. Bajuk-Bogdanović, I. Holclajtner-Antunović, *J. Therm. Anal. Calorim.* **2016**, *126*, 1567 – 1577.

Manuscript received: October 24, 2019
Revised manuscript received: January 20, 2020
Accepted manuscript online: February 11, 2020
Version of record online: March 18, 2020

